# Radiative & Excited State Charmonium Physics

**Jozef J. Dudek**[*][†]

*Jefferson Laboratory MS 12H2, 12000 Jefferson Avenue, Newport News, VA 23606, USA*
*Department of Physics, Old Dominion University, Norfolk, VA 23529, USA*
*E-mail:* `dudek@jlab.org`

Renewed interest in the spectroscopy of charmonium has arisen from recent unexpected observations at $e^+e^-$ colliders. Here we report on a series of works from the previous two years examining the radiative physics of charmonium states as well as the mass spectrum of states of higher spin and internal excitation. Using new techniques applied to Domain-Wall and Clover quark actions on quenched isotropic and anisotropic lattices, radiative transitions and two-photon decays are considered for the first time. Comparisons are made with experimental results and with model approaches. Forthcoming application to the light-quark sector of relevance to experiments like Jefferson Lab's GlueX is discussed.

---

[*]Speaker.

[†]based upon work done in collaboration with R.G.Edwards, N.Mathur and D.G.Richards

## 1. The Charmonium Landscape

Until rather recently, the bulk of experimental knowledge about charmonium spectroscopy lay at energies below or only slightly above the threshold for open charm ($D\bar{D}$) production. This consisted of three vector resonances ($J/\psi, \psi(3686), \psi(3770)$), a pseudoscalar ($\eta_c$) and three states with positive parity and charge conjugation ($\chi_{c0,1,2}$). In addition, measurements had been made of radiative transitions between these states (e.g. $\chi_{c0} \to J/\psi\gamma$) and of the two-photon decays of the $\eta_c, \chi_{c0,2}$. The only knowledge of states above $D\bar{D}$ threshold came from badly-constrained fits to inclusive $e^+e^-$ cross-sections yielding a tentative excited vector meson spectrum. Overall these observations have been described well by quantum-mechanical models in which charm quarks move non-relativistically in an assumed potential.

In the current century the charmonium picture has filled out considerably and new mysteries have arisen owing to the high statistics and new production methods made possible by CLEO-c and the *B*-factories. The remaining expected sub-threshold states, $\eta'_c, h_c$, have been observed, as have radiative transitions from the $\psi(3770)$ down to the $\chi_{cJ}$. The above-threshold spectrum is rapidly being mapped[1], with some states living up to the expectations of potential models[2] and others coming as something of a surprise[3]. The increasingly complete set of exclusive data in $e^+e^-$ looks set to allow determination of the vector spectrum with some confidence.

In a series of recent works[4, 5, 6], members of the JLab lattice group have investigated the possibility of computing several of these quantities using lattice QCD. These initial studies have been carried out on quenched lattices with rather promising results. In the sections that follow I will briefly describe the work done.

## 2. Radiative Transitions

One motivation for investigating the coupling of photons to meson states is to extract photocouplings for use in studies of meson photoproduction. At Jefferson Lab this is of particular interest with the likely future running of the GlueX experiment which will photoproduce light mesons using a 9 GeV photon beam. Indications from models[7, 8] have been that there should be unsuppressed production of previously unobserved exotic hybrid mesons in such a process. A firmer prediction using lattice QCD is an aim of the JLab lattice group.

Validating any new lattice radiative technique in the light meson sector is rendered difficult by the sparsity of good radiative data (something that GlueX aims to remedy), and as such it was decided to initially investigate methods in the charmonium sector. Here, as well as there being good data to compare with, there are also fewer (or at least different) lattice technical constraints - signals are typically cleaner, boxes can be smaller and no extrapolation in charm quark mass should be required.

In [4], the JLab group applied an ambitious combination of lattice techniques, computing three-point functions with heavy domain wall fermions on an anisotropic lattice ($\xi = 3$ at $a_s \sim 0.1\,\mathrm{fm}$) within the quenched approximation. Anisotropic lattices as applied to charmonium exploit the fact that while the quark mass scale demands a cut-off above $\sim 1.5$ GeV, the internal three-momentum scale is typically much lower, $\sim 500$ MeV. On the lattice used, we can have both $m_c a_t$

and $|\vec{p}|a_s$ reasonably small and a spatial box size $\gtrsim 1$ fm without requiring very many spatial lattice sites.

Three-point functions were computed using local fermion bilinears as interpolating fields, thus limiting the states that can be considered to the set of quantum numbers $0^{\pm+}, 1^{\pm-}, 1^{++}$. The sequential source technique was utilised, allowing without additional cost insertion of any current or momentum, but requiring a new computation for each sink operator or momentum change. Disconnected diagrams were not included.

Relating the three-point functions to transition form-factors requires knowledge of the overlap of operators on to states (e.g. $Z = \langle \chi_{c0} | \bar{\psi}\psi(0) | 0 \rangle$), the mass spectrum and a decomposition of the matrix elements of the vector current. As an example of the latter, consider the following covariant decomposition between a scalar (e.g. $\chi_{c0}$) and a vector (e.g. $\psi$):

$$\langle S(\vec{p}_S) | j^\mu(0) | V(\vec{p}_V, r) \rangle = \Omega^{-1}(Q^2) \left( E_1(Q^2) \left[ \Omega(Q^2)\varepsilon^\mu(\vec{p}_V, r) - \varepsilon(\vec{p}_V, r).p_S \left( p_V^\mu p_V.p_S - m_V^2 p_S^\mu \right) \right] \right.$$
$$\left. + \frac{C_1(Q^2)}{\sqrt{q^2}} m_V \varepsilon(\vec{p}_V, r).p_S \left[ p_V.p_S(p_V + p_S)^\mu - m_S^2 p_V^\mu - m_V^2 p_S^\mu \right] \right),$$

where $\Omega(Q^2)$ is an invariant function. Here there are two possible transition form-factors, $E_1(Q^2)$ which corresponds to the electric dipole multipole of a transverse photon and $C_1(Q^2)$ which occurs only for a longitudinal photon and hence vanishes as $Q^2 \to 0$. The non-conserved local vector current was used in this study, with the multiplicative renormalisation constant set by insisting that the $Q^2 = 0$ "form-factor" of the $\eta_c$ was 1.

Given knowledge of the $Z$, $E$, one can cast the extraction of the form-factors as the solution of an overconstrained linear system to be solved at each value of $Q^2$ allowed by lattice kinematics.

By analogy to the electromagnetic form-factors of the proton, pion and other hadrons, one can define form-factors for charmonia. However charmonia are states of definite charge conjugation and as such do not have electromagnetic form-factors (the photon has $C = -1$), but one can still define a single-quark form-factor by coupling the vector current only to the quark field. This will yield information about the quark distribution within the state. In the case of the $\eta_c$, whose form-factor decomposition is the same as that of the pion, we extract the data shown in figure1(a).

The first thing we note is that unlike the pion case, the form-factor is not well described by vector dominance of the lightest vector resonance (here the $J/\psi$ - with the imperfect quark mass tuning we used this has mass 2.9 GeV on this lattice) . This can be understood by comparing the complex $Q^2$ plane in the two cases - in the pion case the $\rho$ meson is the closest timelike singularity (neglecting the effect of multiparticle cuts) with the next nearest, the excited $\rho(1460)$ being relatively rather distant and hence having a much reduced effect. In the charmonium case, the vector resonances are comparable distances from the spacelike region and can all be expected to contribute. This suggests that parameterising the form-factor in terms of vector meson contributions will be rather inefficient.

Instead we fit the lattice data with a simple analytic form $f(Q^2) = \exp\left[ -\frac{Q^2}{16\beta^2}(1 + \alpha Q^2) \right]$, yielding $\beta = 480(3)$ MeV, $\alpha = -0.046(1)$ GeV$^{-2}$ and what is clearly a good fit. This corresponds to a "charge radius" of $\sqrt{\langle r^2 \rangle} = 0.25$ fm, giving some a posteriori justification for the lattice size being only $\sim 1.2$ fm. This form-factor can be computed in potential models where it corresponds
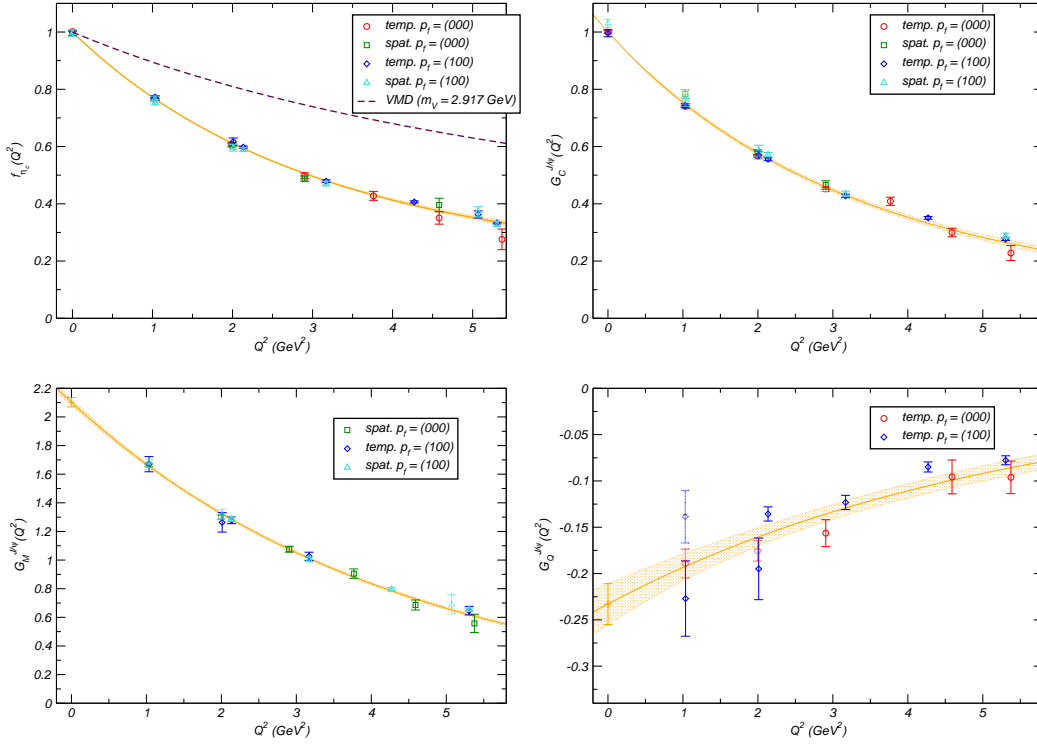
**Figure 1:** (a) $\eta_c$ form-factor (b) $J/\psi$ 'charge' form-factor (c) $J/\psi$ 'magnetic dipole' form-factor (d) $J/\psi$ 'electric quadrupole' form-factor

to wavefunction overlap with a vector current insertion, but since these models are not covariant it suffers from a frame ambiguity[9].

Results for the $J/\psi$ which, like the vector deuteron, has three form-factors are shown in figures 1(b,c,d). We note that the "charge radius" is compatible with that found for the $\eta_c$ which is in line with the idea that they have the same spatial wavefunctions up to small spin-dependent effects. The value of the magnetic dipole form-factor at $Q^2 = 0$ indicates that non-perturbative gluon effects do not give rise to an effective anomalous magnetic moment for the charm quark as had been suggested earlier[10]. The small magnitude of the quadrupole form-factor limits the size of gluonic tensor-forces between charm quarks in potential models. The extracted form-factor for the $\chi_{c0}$ is described by a larger "charge radius" of $\sim 0.3\,\mathrm{fm}$ which within a potential model is explained by the state having a $P$-wave between the charm quarks.

The transition with least statistical noise on the lattice signal is $J/\psi \to \eta_c\gamma$. However in this channel there are problems with both the lattice extraction and the experimental value. The experimental value of $\Gamma(J/\psi \to \eta_c\gamma)$ quoted by the PDG[11] comes from a single experiment, namely Crystal Ball[12]. It has never been confirmed and is known to be rather sensitive to a number of factors, including a difficult experimental background, and the badly known total width of the $\eta_c$[13]. Most models, unless tuned to accommodate it, do not agree with the quoted value. A sophisticated analysis at CLEO-c to extract this number with realistic systematic error estimation is underway.

From the lattice side, we have the problem that the hyperfine splitting, which sets the phase space for this transition, is not well determined. It is only with dynamical lattices and improved actions that one comes close[14]. We demonstrate this ambiguity by showing in figure 2 the experimental width converted to a matrix element at $Q^2 = 0$ in two ways, dividing out either the physical phase-space or the phase-space corresponding to our lattice estimate of the hyperfine splitting.
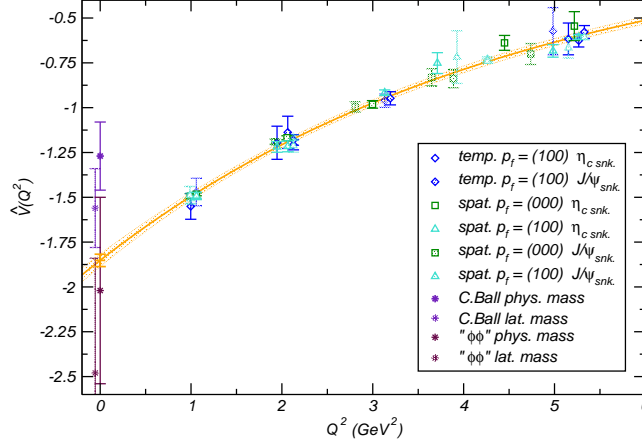


**Figure 2:** $J/\psi \to \eta_c \gamma$ transition form-factor

We see in figure 2 that the lattice kinematics do not provide a datum at $Q^2 = 0$ and we are forced to extrapolate. We use a simple exponential form $\hat{V}(Q^2) = \hat{V}(0) \exp\left[-\frac{Q^2}{16\beta^2}\right]$ that fits the data well.

A channel with reasonable noise, little phase space ambiguity and relatively precise experimental data is the electric dipole transition $\chi_{c0} \to J/\psi \gamma$. In figure 3(a) we show our results. The data is fitted with the form $\hat{E}_1(Q^2) = \hat{E}_1(0)\left(1 + \frac{Q^2}{\rho^2}\right) \exp\left[-\frac{Q^2}{16\beta^2}\right]$. The slightly timelike data allowed by the lattice kinematics is not included in the fit, so the fact that the curve extrapolates through these points is a non-trivial test of its suitability. The agreement with the experimental data is reasonable. Shown in figure 3(b) is the longitudinal multipole $C_1(Q^2)$.

In the transition $\chi_{c1} \to J/\psi \gamma$, two multipoles persist as $Q^2 \to 0$, an electric dipole and a magnetic quadrupole. In non-relativistic theories the quadrupole is much suppressed and has a magnitude which is very sensitive to the approximations made within the model. Experimentally the two multipoles can be separated by studying the angular distribution of the photon in the decay. In the lattice extraction, all independent multipole amplitudes are extracted simultaneously when we solve the linear system of three-point functions. Results are presented in [4].

One motivation for the fit forms we have used in the case of electric dipole transitions comes from potential models in which the spatial wavefunctions are approximated by those of the harmonic oscillator potential. In this case, including spin-dependent corrections to the lowest order electric dipole operator one obtains

$$E_1^{\mathrm{QM}}(Q^2) = a\left(1 + r\frac{|\vec{q}|^2}{4\beta_\psi^2}\right)\exp{-\frac{|\vec{q}|^2}{16\bar{\beta}^2}} \approx E_1^{\mathrm{QM}}(0)\left(1 + r\frac{Q^2}{4\beta_\psi^2}\right)\exp{-\frac{Q^2}{16\bar{\beta}^2}},$$
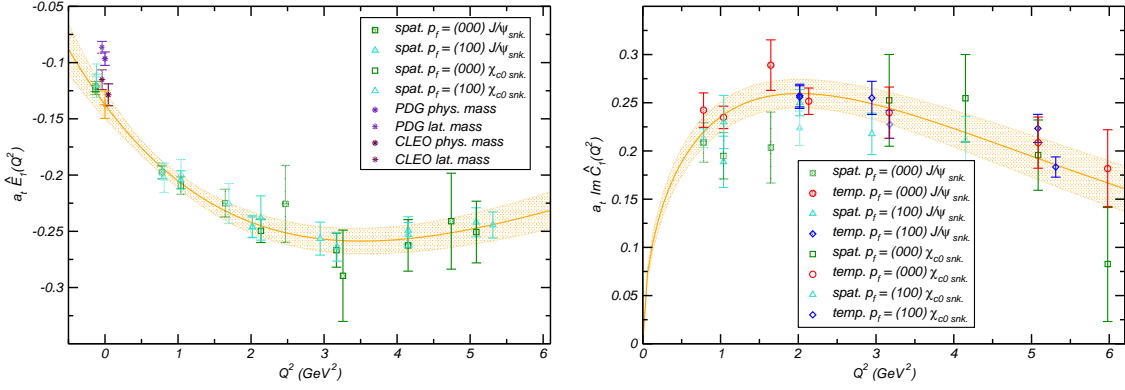
**Figure 3:** $\chi_{c0} \to J/\psi\gamma$ transition form-factors (a) $E_1$ (b) $C_1$

where $r$ is related to spin-orbit Clebsch-Gordan coefficients, $r = 2\,(\chi_{c0})$, $1\,(\chi_{c1})$, $0\,(h_c)$, and where this is evaluated in the $\chi_c$ rest frame at small $Q^2$. Hence, to a first approximation we'd expect that $\rho \sim \frac{1}{\sqrt{r}}$ so that $\rho(\chi_{c1}) \approx \sqrt{2}\rho(\chi_{c0})$ and $\rho(h_c) \to \infty$. In the same approximation we have $\rho(\chi_{c0}) \approx 2\beta_\psi$. Within the large errors on the lattice results, these relations appear to be satisfied.

## 3. Two-Photon Decays

Charmonium states of positive charge conjugation can undergo decay to two photons. Indeed the time-reverse of this process, two-photon fusion, is a commonly used charmonium production method.

Looking naively it is not clear that one can easily evaluate the matrix element for the decay of a hadron to two-photons in lattice QCD. The method used previously for the radiative transition worked because in the limit of large Euclidean time separation, the interpolating fields at source and sink overlapped only with the lightest QCD eigenstates of the appropriate quantum numbers - the vector current insertion between them initiating the transition between orthogonal states. In the two-photon case, one external particle must be a photon. If we guessed that a vector current would serve as an interpolating field for a photon, we would find a large time separations that we actually overlapped with the $J/\psi$[1]. The problem is that a photon is not an eigenstate of QCD. The solution comes when one realises that the photon is, however, a superposition of QCD eigenstates, with this defined precisely by the field-theoretic Lehmann-Symansik-Zimmerman reduction.

The connection between the LSZ reduction and external photons in the specific case of Lattice QCD was first expressed in [15], where it was applied to the hadronic structure of the photon. In [5] the method was demonstrated for the two-photon decays of the $\eta_c$ and the $\chi_{c0}$. Here we outline

---

[1]in this quenched study without disconnected diagrams

the method beginning with the LSZ reduction of the amplitude in the QCD+QED theory,

$$\langle \gamma(q_1, \lambda_1) \gamma(q_2, \lambda_2) | M(p) \rangle =$$
$$- \lim_{\substack{q_1' \to q_1 \\ q_2' \to q_2}} \varepsilon_\mu^*(q_1, \lambda_1) \varepsilon_\nu^*(q_2, \lambda_2) \times q_1'^2 q_2'^2 \int d^4 x d^4 y\, e^{iq_1' \cdot y + iq_2' \cdot x} \langle 0 | T \{ A^\mu(y) A^\nu(x) \} | M(p) \rangle,$$

up to photon renormalisation factors. The explicit photon fields prevent direct computation of this quantity in pure lattice QCD, however we can utilize the perturbative expansion of the photon-quark coupling to approximately integrate them out (the path-integral over gluon fields is suppressed):

$$\int \mathscr{D}A \mathscr{D}\bar\psi \mathscr{D}\psi\, e^{iS_{QED}[A,\bar\psi,\psi]} A^\mu(y) A^\nu(x) =$$
$$\int \mathscr{D}A \mathscr{D}\bar\psi \mathscr{D}\psi\, e^{iS_0[A,\bar\psi,\psi]} \left( \ldots + \frac{e^2}{2} \int d^4 z d^4 w \left[ \bar\psi \gamma^\rho \psi A_\rho \right](z) \left[ \bar\psi \gamma^\sigma \psi A_\sigma \right](w) + \ldots \right) A^\mu(y) A^\nu(x),$$

The integration over the photon field can be carried out by Wick contracting the fields into propagator products, so that, neglecting disconnected pieces,

$$\langle \gamma(q_1, \lambda_1) \gamma(q_2, \lambda_2) | M(p) \rangle = (-e^2) \lim_{\substack{q_1' \to q_1 \\ q_2' \to q_2}} \varepsilon_\mu^*(q_1, \lambda_1) \varepsilon_\nu^*(q_2, \lambda_2) q_1'^2 q_2'^2$$
$$\times \int d^4 x d^4 w d^4 z\, e^{iq_1' \cdot x} D^{\mu\rho}(0, z) D^{\nu\sigma}(x, w) \langle 0 | T \{ j_\rho(z) j_\sigma(w) \} | M(p) \rangle.$$

The photon propagator can be written $D^{\mu\nu}(0, z) = -ig^{\mu\nu} \int \frac{d^4 k}{(2\pi)^4} \frac{e^{ik.z}}{k^2 + i\varepsilon}$, cancelling the inverse propagators outside the integral and supplying some momentum-conserving delta functions.

As explained in [15], the resulting expression can be analytically continued from Minkowski to Euclidean space-time provided the photon virtualities, $Q_1^2 = |\vec{q}_1|^2 - \omega_1^2$, $Q_2^2 = |\vec{q}_2|^2 - \omega_2^2$ are not sufficiently timelike that they can produce on-shell hadrons. In charmonium[2] this limits us to $Q^2 > -m_{J/\psi}^2$. Using suitable a QCD interpolating field to produce $M$ and reversing the operator time-ordering for convenience we have

$$\langle M(p) | \gamma(q_1, \lambda_1) \gamma(q_2, \lambda_2) \rangle = \lim_{t_f - t \to \infty} e^2 \frac{\varepsilon_\mu(q_1, \lambda_1) \varepsilon_\nu(q_2, \lambda_2)}{\frac{Z_M(p)}{2E_M(p)} e^{-E_M(p)(t_f - t)}}$$
$$\times \int dt_i\, e^{-\omega_1(t_i - t)} \langle 0 | T \left\{ \int d^3 \vec{x}\, e^{-i\vec{p}.\vec{x}} \varphi_M(\vec{x}, t_f) \int d^3 \vec{y}\, e^{i\vec{q}_2.\vec{y}} j^\nu(\vec{y}, t) j^\mu(\vec{0}, t_i) \right\} | 0 \rangle \quad (3.1)$$

It is clear from the previous discussion that obtaining two-photon widths is a natural extension to the study of radiative transitions carried out in [4] - there we computed three-point functions involving vector currents with the source ($t_i$) and sink ($t_f$) positions fixed and varied the vector current "insertion" ($t$) across the temporal direction to plot out a plateau. For two-photon widths we repeat this but with a varying sink (or in the case of eqn. (3.1), source) position which will be integrated over with an exponential weighting.

---

[2]This is true within the quenched truncation, neglecting disconnected diagrams. Relaxing these approximations allows production of light vector mesons, multi-pion states or vector glueballs - phenomenologically we expect these states to have small coupling to the charmonium meson

Calculations were performed on $24^3 \times 48$ *isotropic* quenched lattices with a lattice spacing $a \approx 0.047$ fm (determined from the static quark potential in [16]). The charm quarks were described by a non-perturbatively improved Clover action [17] with Dirichlet boundaries in the temporal direction. Given the small "charge radii" found for ground-state charmonia in the previous study, we did not expect significant finite volume effects in this study. We adopted the conserved ("point-split") vector current at the insertion.

We applied two different methods to calculate the two-photon matrix element. The first (using 174 configurations) was to place the meson state at a fixed sink position $t_f = 37$. As in [4] the sink was used as a sequential source for a backward propagator inversion, meaning that its properties were fixed for each computation while we were able, without further cost, to vary the direction and momentum of the insertion and the direction of the source field. We then computed with all possible source positions, $t_i$, which, while costly in computing time, allowed us to freely vary the value of $\omega_1$ and hence $Q_1^2$ and in addition to view the subsequent integrand. In figure 4(a) we display the integrand for "insertion" positions $t = 4, 16, 32$, $\vec{p}_f = (000)$ and $\vec{q}_1 = (100)$ with an $\eta_c$ at the sink.
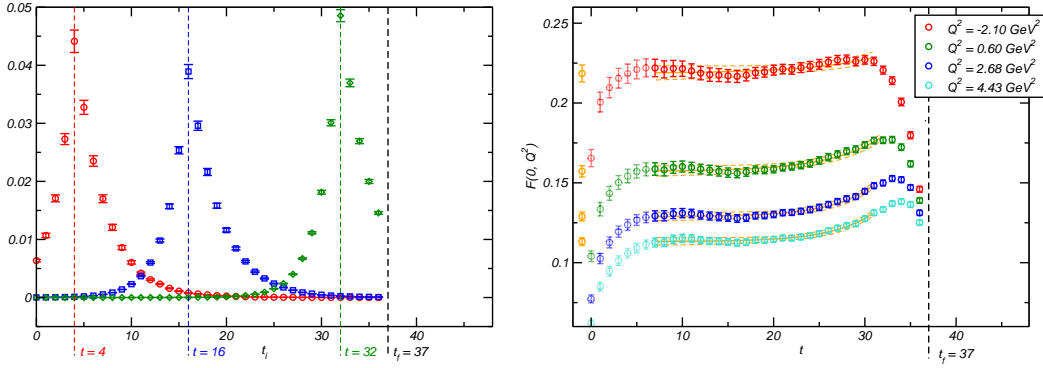


**Figure 4:** (a) Integrand at three values of vector current insertion time ($t = 4, 16, 32$) with pseudoscalar sequential source at sink position $t_f = 37$. (b) Pseudoscalar two-photon form-factor as a function of time slice, $t$. First six time slices ghosted out due to the Dirichlet wall truncating the integral. Constant plus single exponential fits shown in orange.

In principle there can be a contact term when the two vector currents are on the same timeslice - while there is not a clear signal of this in the data, this point requires further study.

It is clear that provided the insertion is not placed too close to the Dirichlet wall (i.e. $t \gtrsim 7$) we will be able to capture the full integral by summing time slices, $t_i$. The integral as a function of insertion position $t$ is shown in figure 4(b) for a selection of $Q_2^2$ with $Q_1^2 = 0$ ($\omega_1 = |\vec{q}_1|$) where we observe plateaus with the deviation from plateau behavior at larger $t$ coming from excited $\eta_c$ contributions, both of which are fitted simultaneously. Extracting the plateau values for a range of $Q_1^2$ (which we are free to choose continuously) and $Q_2^2$ (which is fixed for a given set of $\omega_1, \vec{q}_2, \vec{p}$), we find the dependence displayed in figure 5. We plot dimensionless $F$ defined by $\langle \eta_c | \gamma(q_1, \lambda_1) \gamma(q_2, \lambda_2) \rangle = 2(\frac{2}{3}e)^2 m_{\eta_c}^{-1} F(Q_1^2, Q_2^2) \varepsilon_{\mu\nu\rho\sigma} \varepsilon_1^\mu \varepsilon_2^\nu q_1^\rho q_2^\sigma$, where the on-shell decay width is $\Gamma(\eta_c \to \gamma\gamma) = \pi \alpha_{em}^2 \frac{16}{81} m_{\eta_c} |F(0,0)|^2$.

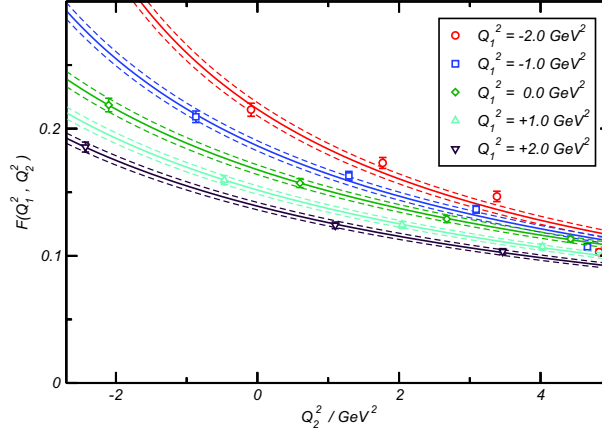**Figure 5:** $\eta_c$ two-photon form-factor, $F(Q_1^2, Q_2^2)$. Points are lattice QCD data, fits are monopole forms as described in [5] .

The method of computing three-point functions with all possible source positions ($t_i = 0 \ldots t_f$) is extremely costly in computing resources. With the penalty of losing the ability to freely vary $Q_1^2$ we can reduce the computing time by a factor of $\mathcal{O}(L_t)$ by putting the meson interpolating field at the (fixed) source position and using

$$\int dt \, e^{\omega_1 t} \int d^3\vec{z} \, e^{i\vec{q}_1 \cdot \vec{z}} \bar{\psi}(\vec{z}, t) \gamma^\mu \psi(\vec{z}, t)$$

in the sequential source for the backward propagator inversion. It is then necessary to fix $\omega_1$ and $\vec{q}_1$ in advance and one cannot view the integrand since the integration is being performed "on-the-fly" within the sequential source. We computed 300 configurations with $Q_1^2 = 0$ in this way and the results for $\eta_c$ and $\chi_{c0}$ are displayed in figure 6, where we define the $\chi_{c0}$ two-photon form-factor by

$$\langle \chi_{c0} | \gamma(q_1, \lambda_1) \gamma(q_2, \lambda_2) \rangle = 2(\tfrac{2}{3}e)^2 m_{\chi_{c0}}^{-1} G(Q_1^2, Q_2^2) \big( \varepsilon_1 \cdot \varepsilon_2 q_1 \cdot q_2 - \varepsilon_2 \cdot q_1 \varepsilon_1 \cdot q_1 \big).$$
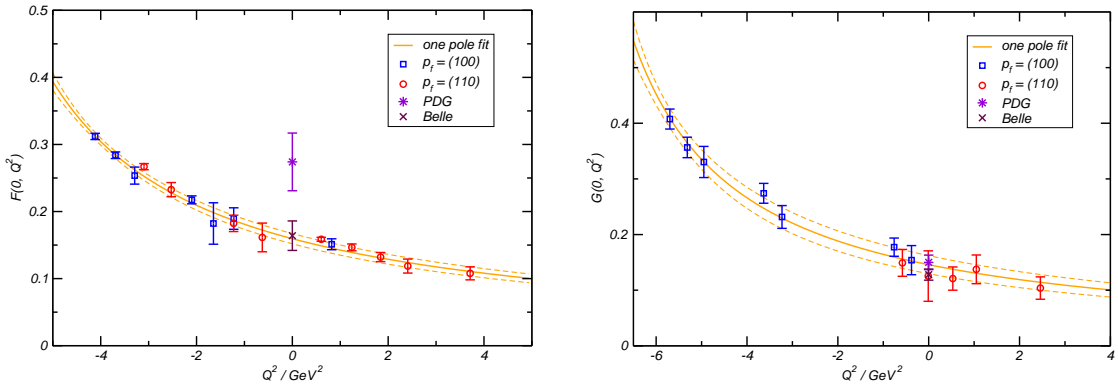


**Figure 6:** (a) $\eta_c \to \gamma\gamma^*$ form-factor (b) $\chi_{c0} \to \gamma\gamma^*$ form-factor. Experimental numbers extracted from the PDG and a recent Belle preprint[18]

Of course here the errors displayed on the lattice data are statistical only and must be augmented by an uncertainty due to scaling from our fixed lattice spacing to the continuum and one related to the lack of light-quark loops within the quenched truncation. This is the first demonstration of this method, such controlled studies will doubtless follow now that efficacy has been demonstrated.

## 4. Higher Excitations

In the previous two section I reported on radiative results involving charmonia that are the lightest state in a given $J^{PC}$. There is also good data on radiative processes involving excited states. The techniques outlined above extend well to excited states if one has a method to determine the energies and overlap factors for the excited states with some degree of reliability. A method that is not particularly reliable is to consider the sub-leading exponential behaviour of two-point correlators, especially in a case like charmonium where for example the vector channel has two near-degenerate first excited states ($\psi(3686)$, $\psi(3770)$).

In [6], the possibility of using a matrix of two-point correlators with a broad range of interpolating fields was investigated. As well as the mass spectrum (for which this method is often used) we also required the overlap factors for later use in converting three-point functions into radiative transition matrix elements.

### 4.1 Operators, their continuum limits and lattice irreps

A operator basis was constructed based upon operators that in the continuum would have the structure of fermion bilinears with a number of symmetric covariant derivatives

$$\mathscr{O}_{\mu\nu\rho\cdots} = \bar{\psi}(x)\Gamma_\mu \overleftrightarrow{D}_\nu \overleftrightarrow{D}_\rho \cdots \psi(x).$$

In the continuum, the overlap of these fields on to states of definite spin can be constructed by insisting upon Lorentz covariance (and imposing the discrete $P$ and $C$ symmetries), e.g.

$$\langle 0|\bar{\psi}(x)\gamma_\mu \overleftrightarrow{D}_\nu \psi(x)|2^{++}(\vec{p},r)\rangle = Z \in_{\mu\nu}(\vec{p},r),$$

where $\in_{\mu\nu}(\vec{p},r)$ is the polarisation tensor for a spin-2 particle with $J_z = r$. The utility of having these decompositions will become clear later.

On a cubic lattice at zero three-momentum, the appropriate symmetry group is not $O(3)$, but rather the cubic group whose irreps are not labelled by an infinite tower of spins, but the finite set $A_1, A_2, E, T_1, T_2$. As is well known, in the continuum these irreps contain multiple spins (see table 1) and this makes the spin-assignment of lattice eigenstates a non-trivial business.

We construct operators that transform irreducibly by projecting out certain linear combinations of the spatial components of our derivative-based operators[3]. For example the $T_2$ and $E$ components of the operator $\bar{\psi}(x)\gamma_\mu \overleftrightarrow{D}_\nu \psi(x)$ shown above are

$$\mathscr{O}_{T_2}^i = |\varepsilon^{ijk}|\bar{\psi}(x)\gamma_j \overleftrightarrow{D}_k \psi(x); \quad \mathscr{O}_E^i = \mathbb{Q}^{ijk}\bar{\psi}(x)\gamma_j \overleftrightarrow{D}_k \psi(x)$$

---

[3]the operators are a corrected extension of those presented in [19]

| $\Lambda$ | $d_\Lambda$ | $J$ |
|---|---|---|
| $A_1$ | 1 | $0, 4, 6, \ldots$ |
| $A_2$ | 1 | $3, 6, 7, \ldots$ |
| $E$ | 2 | $2, 4, 5, \ldots$ |
| $T_1$ | 3 | $1, 3, 4, \ldots$ |
| $T_2$ | 3 | $2, 3, 4, \ldots$ |

**Table 1:** The table shows the single-valued irreducible representations $\Lambda$ of the cubic group $O$, together with their dimensions $d_\Lambda$ and continuum spin content $J$. Additional superscripts are employed to denote charge conjugation $C$ and parity $P$.

where the covariant derivative is approximated by a gauge-covariant finite difference on the lattice and where the $E = T_1 \otimes T_1$ Clebsch-Gordan coefficients are zero except for the elements

$$\mathbb{Q}_{111} = \tfrac{1}{\sqrt{2}}; \ \ \mathbb{Q}_{122} = -\tfrac{1}{\sqrt{2}}; \ \ \mathbb{Q}_{211} = -\tfrac{1}{\sqrt{6}}; \ \ \mathbb{Q}_{222} = -\tfrac{1}{\sqrt{6}}; \ \ \mathbb{Q}_{233} = \tfrac{2}{\sqrt{6}}.$$

If we performed these projections in the continuum theory we would have

$$\langle 0|\mathscr{O}_{T_2}^i|2^{++}(\vec{p}, r)\rangle = Z|\varepsilon^{ijk}| \in_{jk} (\vec{p}, r); \ \ \langle 0|\mathscr{O}_E^i|2^{++}(\vec{p}, r)\rangle = Z\mathbb{Q}^{ijk} \in_{jk} (\vec{p}, r)$$

so that, at zero three-momentum, if we average over the spatial directions in the correlation function $C^{ij} = \langle 0|\mathscr{O}^i\mathscr{O}^j|0\rangle$, we'd have that the $Z$'s extracted from the $T_2, E$ correlators would be related to the common spin-2 particle $Z$ as $Z_{T_2} = \sqrt{2}Z_E = \sqrt{2}Z$. In a lattice simulation at finite $a$ we might hope that we are "sufficiently" close to the continuum that this relation still holds approximately. If it does, we can associate with increased confidence particular states in independent irreps $T_2, E$ with components of the same spin-2 particle[4]. This is particularly important in charmonium where there are true "dynamical" degeneracies that are not lifted as one moves to the continuum limit.

### 4.2 The spectrum extraction method

We basically solve the now familiar generalised eigenvalue problem

$$C(t)v_\alpha = \lambda_\alpha(t)C(t_0)v_\alpha,$$

for the eigenvalues (from which we obtain state masses) and the eigenvectors (from which we obtain the $Z$'s). A novel feature we have implemented is setting the value of the reference time $t_0$ in a systematic way.

Since in practice we work with a finite space of operators, the parameter $t_0$ plays an important role. The eigenvectors are forced by the solution procedure to be orthogonal on the metric $C(t_0)$ - this will only be a good approximation to the true orthogonality (which in the continuum is defined with an infinite number of states and operators) if the correlator at $t_0$ is dominated by the lightest $\dim(C)$ states. As such one should choose $t_0$ large enough that you believe the above statement to be true.

---

[4]The possible effects of divergent operator mixing for higher derivative operators has not yet been fully investigated. In this work we included operators with a maximum of two derivatives.

In choosing a $t_0$ value for a given $C(t)$ there are two factors to take into account - the above discussion suggests we should push $t_0$ out to larger values, where the contributions of higher excited states have decayed exponentially; however, as we do so we get into a region where the correlator data are typically noisier. The noise on $C(t_0)$ will enter into the solution of the eigenvalue problem at all timeslices and as such we do not want to make $t_0$ too large. We need a criterion to decide upon an optimum value of $t_0$ - our choice was to define a chi-squared-like quantity gauging how well the generalized eigenvalue solution (with time-independent $Z$ values) describes the correlators. At a given $t_0$ we solve the eigenvalue problem to yield masses and $Z$'s. With these in hand we can reconstruct any correlator matrix element using the spectral decomposition. A suitable chi-squared-like quantity can be defined as

$$\chi^2 = \frac{1}{\frac{1}{2}N(N+1)(t_{\max}-t_0) - \frac{1}{2}N(N+3)} \sum_{i,j \geq i} \sum_{t,t'=t_0+1}^{t_{\max}} (C_{ij}(t) - C_{ij}^{\mathrm{rec.}}(t)) \mathbb{C}_{ij}^{-1}(t,t') (C_{ij}(t') - C_{ij}^{\mathrm{rec.}}(t')),$$

where $N = \dim(C)$ and where $\mathbb{C}$ is the data correlation matrix for the correlator $C_{ij}$ computed with jackknife statistics.

The optimum value of $t_0$ is chosen to be that which minimizes the chi-squared-like quantity. In fact, since we solve the eigenvalue problem on each timeslice we actually get $Z(t)$; we choose to take the $Z$ values (for a given $t_0$) from a fixed timeslice $t_Z > t_0$ such that the chi-squared-like quantity is minimized at this $t_0$. Since we find that the $Z(t)$ are reasonably flat the chi-squared variation with $t_Z$ is fairly mild. Insisting that the $Z$'s are time independent for $t > t_0$ is a reflection of the fact that the only time-dependence in the spectral representation is in the exponentials.

As a concrete example of our solution scheme, consider the $A_1^{-+}$ channel in which we use an eight-dimensional operator basis. We solve the generalized eigenvalue problem for all $t_0$ between 1 and 10 - the $\chi^2$-like parameter so determined is shown in figure 7, with a clear minimum being observed at $t_0 = 7$. We show in figure 8(a) a typical reconstructed diagonal correlator obtained using the solution at $t_0 = 7$ (and $t_Z = 11$). For comparison in figure 8(b) we show a reconstructed diagonal correlator from the solution with $t_0 = 2$. In the $t_0 = 2$ case $C(t_0)$ is not saturated by the eight states available, and we subsequently force the eigenvectors of $C(t)$ to be orthogonal on the "wrong" metric, a truncated metric belonging to a larger Hilbert space - this shows up at larger times as a poor description of the data.
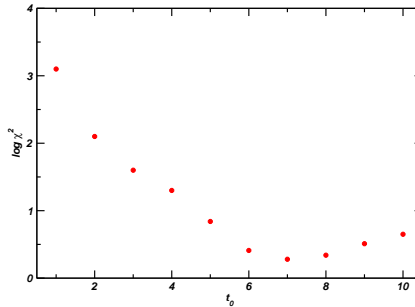


**Figure 7:** Chi-squared-like parameter as a function of $t_0$ for the $A_1^{-+}$ channel.
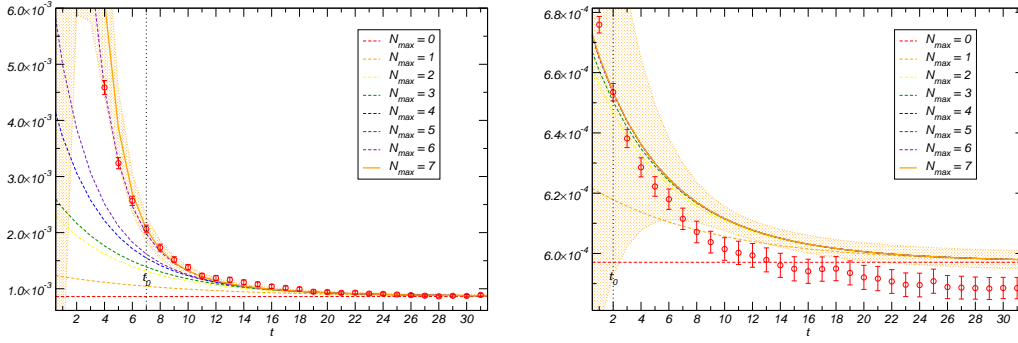
**Figure 8:** (a) Typical reconstructed correlator with optimum $t_0 = 7$. (b) Typical reconstructed correlator with $t_0 = 2$.

Returning to the example reconstructed correlator with $t_0 = 7$, we can see the power of this variational method over more conventional multi-exponential fits. We see that even at timeslice 7 there are at least 6 states contributing considerably to the correlator. It is unlikely that a simple multi-exponential fitter would converge to a solution with a sum of 6 exponentials fitting over the range 7-32. There are approximate degeneracies in the extracted spectrum and in this case the only distinguishing feature of the states are the $Z$'s or equivalently the eigenvectors. Without enforcing orthogonality (as is done in the correlation matrix method) it is hard to see how one would extract meaningful information on these degenerate states.

### 4.3 Spectrum results

Computations were performed using the same quenched anisotropic lattice as where used in the radiative transitions study. In this case an anisotropic clover action was used for the charm quarks, see [6] for details.

### 4.3.1 $J^{++}$

In figure 9(a) we display the states extracted. The lowest band of states, at around 3500 MeV, can be identified with the near-degenerate $\chi_{c0,1,2}$ states. Support beyond simply mass degeneracy[5] for the common $2^{++}$ assignment of the lightest state in $T_2$ and $E$ comes from the extracted $Z$-values. Consider for example the operator $\rho \times \nabla$; this is exactly the operator we presented earlier: $\bar{\psi}(x)\gamma_\mu \overleftrightarrow{D}_\nu \psi(x)$. For the lightest state in $T_2, E$ we find that $\frac{Z_{T_2}}{\sqrt{2}Z_E} = 1.00(1)$. We take this as evidence that these states are rather close to being components of the same $2^{++}$ state. Equivalent analyses can be performed on other operators support this hypothesis.

### 4.3.2 $J^{--}$

This is a very interesting channel in charmonium owing the expected near degeneracy of the $\psi(3686), \psi(3770)$ and an expected $\psi_3$ state which will all appear in the $T_1$ representation. Our

---

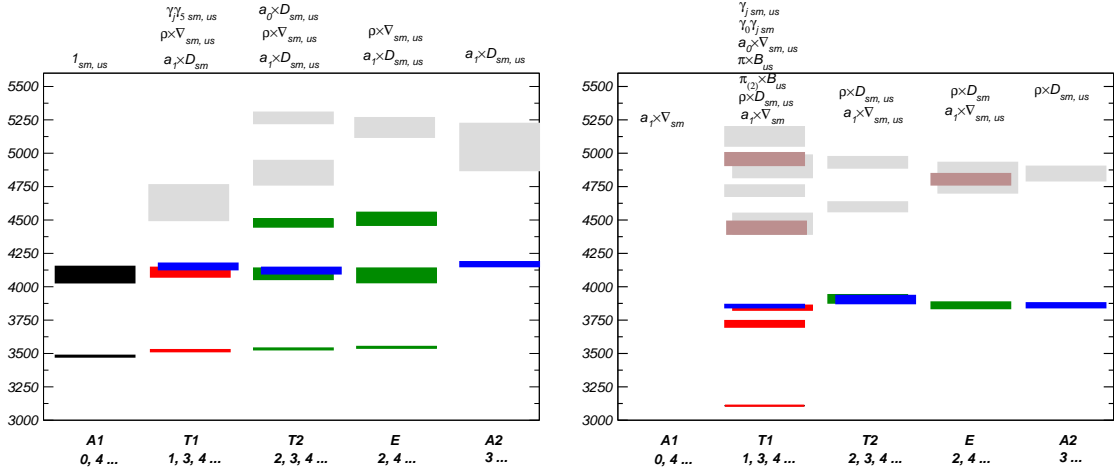[5]this band could belong to a single spin-4 meson

**Figure 9:** (a) $J^{++}$. (b) $J^{--}$. Extracted state masses by zero-momentum lattice irrep. Color coding indicates continuum spin assignment (black=0, red=1, green=2, blue=3, grey=undetermined).

results are presented in figure 9(b). We see precisely the expected behaviour below $4\,\mathrm{GeV}$ in the $T_1$ channel, something we believe has not been hitherto observed in a lattice simulation, and which was only possible because of the state orthogonality implicit in the variational solution method.

### 4.3.3 $J^{+-}$

The $J^{+-}$ sector has the interesting property that all states with $J$-even are exotic in the sense of being inaccessible to a fermion-antifermion bound state. Such states can be constructed from higher Fock states and as such are often described as being "multiquarks" (extra quark degrees of freedom) or "hybrids" (extra gluonic degrees of freedom). Adding an extra pair of charm quarks would take the state mass up to around 6 GeV, which is at the scale of our cutoff and where our quenched non-unitarity might be felt. In the physical spectrum it may be possible for light-quarks to play a non-trivial role, in this quenched study we can say nothing about this possibility. If a non-trivial gluonic field produces exotic quantum numbered states we have hope of seeing it here. We appear to identify an exotic $0^{+-}$ state near $4.5\,\mathrm{GeV}$ and an exotic $2^{+-}$ state near $4.7\,\mathrm{GeV}$. Detailed analysis can be found in [6].

### 4.3.4 $J^{-+}$

The $T_1$ channel here is particularly interesting as it can house a hypothetical $1^{-+}$ exotic meson. Several previous lattice simulations have reported mass results for such a state. However, as is clear from the current data which considers all lattice irreps, it is quite possible that the lightest state in $T_1$ is in fact part of a non-exotic spin-4 meson spread across the $T_1, T_2, E, A_1$ irreps. Indeed the potential models in [20] predict a state in this mass region. Application of the $Z$-comparison method outlined earlier to this case gave inconclusive results. We conclude that it is not possible at this stage to say whether the lightest state in the $T_1$ irrep corresponds to spin 1 or 4 in the continuum.
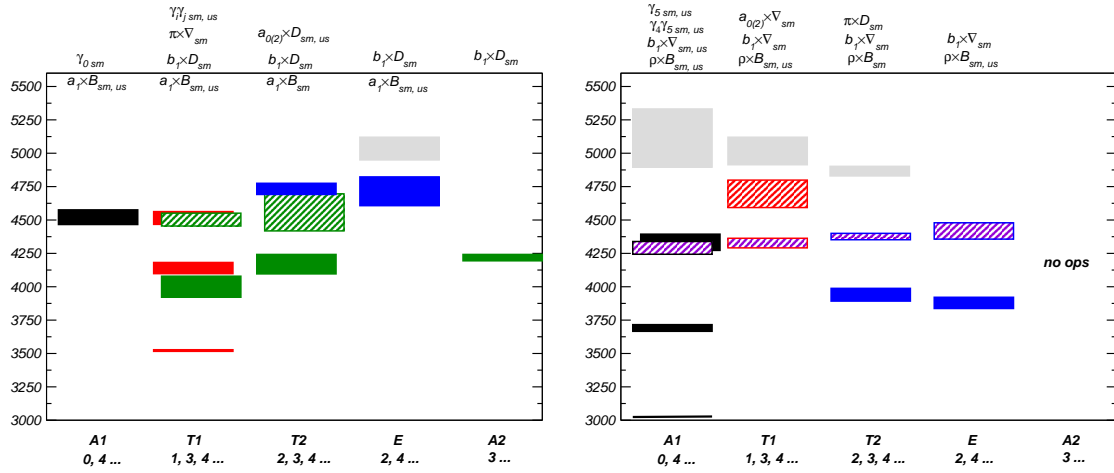
**Figure 10:** (a) $J^{+-}$. (b) $J^{-+}$. Extracted state masses by zero-momentum lattice irrep. Color coding indicates continuum spin assignment (black=0, red=1, green=2, blue=3, grey=undetermined).

## References

[1] E. S. Swanson, Phys. Rept. **429**, 243 (2006), [hep-ph/0601110].

[2] Belle, S. Uehara *et al.*, Phys. Rev. Lett. **96**, 082003 (2006), [hep-ex/0512035].

[3] Belle, S. K. Choi *et al.*, Phys. Rev. Lett. **91**, 262001 (2003), [hep-ex/0309032].

[4] J. J. Dudek, R. G. Edwards and D. G. Richards, Phys. Rev. **D73**, 074507 (2006), [hep-ph/0601137].

[5] J. J. Dudek and R. G. Edwards, Phys. Rev. Lett. **97**, 172001 (2006), [hep-ph/0607140].

[6] J. J. Dudek, R. G. Edwards, N. Mathur and D. G. Richards, arXiv:0707.4162 [hep-lat].

[7] F. E. Close and J. J. Dudek, Phys. Rev. **D69**, 034010 (2004), [hep-ph/0308098].

[8] F. E. Close and J. J. Dudek, Phys. Rev. Lett. **91**, 142001 (2003), [hep-ph/0304243].

[9] O. Lakhina and E. S. Swanson, Phys. Rev. **D74**, 014012 (2006), [hep-ph/0603164].

[10] K. J. Sebastian, H. Grotch and F. L. Ridener, Phys. Rev. **D45**, 3163 (1992).

[11] Particle Data Group, W. M. Yao *et al.*, J. Phys. **G33**, 1 (2006).

[12] J. Gaiser *et al.*, Phys. Rev. **D34**, 711 (1986).

[13] M. Shepherd and R. Mitchell, Private communication, 2007.

[14] HPQCD, E. Follana *et al.*, Phys. Rev. **D75**, 054502 (2007), [hep-lat/0610092].

[15] X.-d. Ji and C.-w. Jung, Phys. Rev. Lett. **86**, 208 (2001), [hep-lat/0101014].

[16] R. G. Edwards, U. M. Heller and T. R. Klassen, Nucl. Phys. **B517**, 377 (1998), [hep-lat/9711003].

[17] M. Luscher, S. Sint, R. Sommer, P. Weisz and U. Wolff, Nucl. Phys. **B491**, 323 (1997), [hep-lat/9609035].

[18] Belle, S. Uehara *et al.*, arXiv:0706.3955 [hep-ex].

[19] X. Liao and T. Manke, hep-lat/0210030.

[20] T. Barnes, S. Godfrey and E. S. Swanson, Phys. Rev. **D72**, 054026 (2005), [hep-ph/0505002].